JGR Oceans

RESEARCH ARTICLE

10.1029/2024JC022246

Observations of Water Mass Modification and Cross-Shelf Exchange at Narsaq Trough, Greenland

Monica Nelson[1], Fiamma Straneo[1,2], Sarah G. Purkey[1], Amy F. Waterhouse[1], Kristen E. Fogaren[3], and Daniel J. Torres[4]

[1]Scripps Institution of Oceanography, University of California San Diego, San Diego, CA, USA, [2]Harvard University, School of Engineering and Applied Sciences, Cambridge, MA, USA, [3]Department of Earth and Environmental Sciences, Boston College, Chestnut Hill, MA, USA, [4]Woods Hole Oceanographic Institution, Woods Hole, MA, USA

Key Points:

- Narsaq Trough steers surface currents on the shelf around the trough and drives a sub-surface cyclonic circulation inside the trough
- Mid-depth waters in Narsaq Trough are fresher, oxygen-enriched, and nutrient-depleted relative to waters at the same depth off the shelf
- Enhanced mixing in the trough suggests that the inflowing waters are modified while circulating around the trough

Supporting Information:

Supporting Information may be found in the online version of this article.

Correspondence to:

M. Nelson,
m3nelson@ucsd.edu

Citation:

Nelson, M., Straneo, F., Purkey, S. G., Waterhouse, A. F., Fogaren, K. E., & Torres, D. J. (2025). Observations of water mass modification and cross-shelf exchange at Narsaq Trough, Greenland. *Journal of Geophysical Research: Oceans*, *130*, e2024JC022246. https://doi.org/10.1029/2024JC022246

Received 19 DEC 2024
Accepted 25 APR 2025

Author Contributions:

Conceptualization: Monica Nelson, Fiamma Straneo, Sarah G. Purkey, Amy F. Waterhouse
Data curation: Fiamma Straneo, Amy F. Waterhouse, Kristen E. Fogaren, Daniel J. Torres
Formal analysis: Monica Nelson, Amy F. Waterhouse
Funding acquisition: Fiamma Straneo
Investigation: Monica Nelson, Fiamma Straneo
Methodology: Monica Nelson, Fiamma Straneo, Sarah G. Purkey, Amy F. Waterhouse

Abstract Cross-shelf exchange at Greenland's continental margins transports warm waters toward the glacier margins and freshwater offshore into the convective basins of the North Atlantic and Nordic Seas. Several studies have suggested that the exchange is enhanced by the presence of deep, glacial troughs, but observations from Greenland's troughs are scarce. This work presents data from a ship-based survey at Narsaq Trough, a wide, branched trough in southwest Greenland, during the summer of 2022. We use Conductivity-Temperature-Depth-Oxygen profiles, water samples for nutrient analysis, and underway current profiles to compare the water mass properties and distribution inside and outside the trough, describe the flow-field in and around the trough, and estimate mixing in the trough. Narsaq Trough is found to provide a pathway for warm, salty Atlantic Water to intrude onto the continental shelf where these waters are mixed with the overlying cold, fresh Polar Water. As a result, waters in the trough are fresher, oxygen-enriched, macronutrient-depleted, and at times colder, relative to the unmodified Atlantic Water offshore. This trough-modified water has the potential to freshen and oxygenate the flow on the shelf-break and/or reduce the thermal forcing of waters in the adjacent fjord, limiting ice melt.

Plain Language Summary Warm, salty waters and cold, fresh waters flow side by side around Greenland, the exchanges of which are important for global climate: Warm, offshore waters reaching the coast effects melt rates of the Greenland Ice Sheet and fresh, onshore waters reaching the open ocean effects stratification, limiting deep ocean mixing. The exchange of these waters is likely affected by troughs (deep grooves in the continental shelf that connect fjords to the open ocean), as is seen in Antarctica, but there is little observational data from troughs in Greenland to confirm this. Here, we use data from a ship-based survey at Narsaq Trough in southwest Greenland to understand how the trough modifies the local environment. Narsaq Trough is found to drive transport both on- and off-shore, with mixing in the trough creating waters that are fresher, oxygen-enriched, nutrient-depleted, and at times colder, relative to the water offshore. This implies that, depending on the fate of the modified water, mixing in troughs could dampen the amount of ice melt resulting from the onshore transport of warm waters and/or could freshen and oxygenate the flow at the edge of the continental shelf.

1. Introduction

At the Greenland continental shelf-break warm, salty Atlantic Water abuts cold, fresh Polar Water. The Atlantic Water is found offshore, largely separated from the Polar Water by the dynamic boundary of the current system and topography of the shelf-break. The rate of cross-shelf exchange in the region controls the net exchange of freshwater offshore and heat onshore, with climatically important impacts. First, freshwater transport offshore affects vertical stratification in the convective basins of the subpolar North Atlantic and is projected to contribute to the slowdown of the Atlantic Meridional Overturning Circulation in a warming climate (Bakker et al., 2016; Rahmstorf et al., 2015; Schiller-Weiss et al., 2024; Swingedouw et al., 2022). Second, heat transport onshore determines the ocean thermal forcing experienced by marine-terminating glaciers that drain the Greenland Ice Sheet and thus affects sea level rise (Slater & Straneo, 2022; Straneo & Heimbach, 2013; Sutherland et al., 2013; Wood et al., 2021). While cross-shelf exchange is known to be driven by eddies and wind stress (Castelao et al., 2019; Snow et al., 2023), the rate may be enhanced by the presence of numerous troughs on Greenland's continental shelf (Snow et al., 2021, 2023; Sutherland & Cenedese, 2009).

Troughs of different sizes, orientations, and geometries incise the continental shelf all around Greenland (Figure 1a). These troughs are deep gouges, carved by glaciers during past glacial periods, extending from the

Project administration: Fiamma Straneo
Software: Amy F. Waterhouse
Supervision: Fiamma Straneo, Sarah G. Purkey
Visualization: Monica Nelson
Writing – original draft: Monica Nelson
Writing – review & editing: Monica Nelson, Fiamma Straneo, Sarah G. Purkey, Amy F. Waterhouse, Kristen E. Fogaren, Daniel J. Torres

mouths of fjords toward the shelf-break (Arndt et al., 2015; Evans et al., 2009). These bathymetric features provide a pathway for deeper waters to access the inner-shelf (Morlighem et al., 2017).

Additionally, a number of prior studies, mostly in Antarctica, have shown that troughs modify their local environment and contribute to cross-shelf exchange. When flow encounters a trough, bathymetric steering can deflect the current, both above and below the shelf, and set up eddies within the trough (Beardsley et al., 2004; Silvano et al., 2022; St-Laurent et al., 2013; Sutherland & Cenedese, 2009). Eddies, wind-reversals, and breaking Rossby waves drive episodic injections of warm water onshore at troughs (Brearley et al., 2019; Moffat et al., 2009; Snow et al., 2023; St-Laurent et al., 2013). Inside Antarctic troughs, mixing is known to drive an upward flux of heat and salt, which cools and freshens the intruded water (Klinck, 1998). This mixing can result from velocity shear created by wind-driven currents and flow encountering topography (Brearley et al., 2017; S. L. Howard et al., 2004; Scott et al., 2021; Venables et al., 2017). As such, troughs in Antarctica are known to be an effective pathway for moving warm water toward the coast and across the pycnocline (Couto et al., 2017; Moffat & Meredith, 2018). In Greenland, the shallower continental shelves generally contain a single cold, fresh layer (Le Bras et al., 2018; Pacini et al., 2021); whereas the deeper continental shelves in Antarctica can support a two-layer system with warmer off-shelf waters underlying the cold shelf waters, even outside of troughs (Moffat & Meredith, 2018). As such, troughs in Greenland may play a greater role in enabling warm, salty waters to access the shelf region than Antarctic troughs.

Hypotheses about the role of troughs on the Greenland shelf can be further developed based on knowledge of submarine canyons. Here, we consider troughs to be bathymetric features carved by glaciers, stretching from the coast across the shelf; whereas canyons are formed through erosion at the shelf-break, cutting down and back from the shelf-break (Harris & Whiteway, 2011; Shepard, 1981). Like canyons, we expect dynamically wide troughs (trough width greater than the radius of deformation), such as Narsaq Trough (30 km > ∼10 km), to steer the flow to follow bathymetry and drive vertical velocities inside the trough (Allen & Hickey, 2010; Freeland & Denman, 1982; Klinck, 1996; Spurgin & Allen, 2014). For the Greenland case, where the troughs are right-bounded (incident flow has the coast to the right) and the pressure gradient is offshore, canyon theory suggests the flow will be steered into the trough along the upstream wall, decelerate, and be pushed deeper by the reduced Coriolis acceleration. On the downstream wall, the flow is steered back out of the trough and accelerated by the pressure gradient, increasing the Coriolis acceleration and lifting the flow back up. However, unlike canyons which are typically deepest at the mouth, troughs often have a shallow sill-type feature at the mouth which impedes the exchange between off-shelf waters and the deepest waters in the trough (Moffat & Meredith, 2018).

A handful of studies (e.g., Snow et al., 2021, 2023; Sutherland & Cenedese, 2009) suggest that Greenland troughs enhance cross-shelf exchange and modify water properties on the shelf. However, limited observations from Greenland's continental margins have made it difficult to confirm their role and understand the local trough dynamics. Here we present novel physical and biogeochemical data from a ship-based survey of Narsaq Trough, in southwest Greenland, to describe how the bathymetric feature steers flow, drives cross-shelf exchange, and modifies Atlantic Water through enhanced mixing.

1.1. Study Region: Narsaq Trough

Narsaq Trough is a wide, branched trough in southwest Greenland, located near the city of Qaqortoq (formerly Julianehåb) and bracketed by Cape Farewell and Cape Desolation (Figure 1b). The trough is 30 km wide at its mouth, narrowing to 25 km before splitting into two branches. It spans the width of the continental shelf, approximately 50 km. The trough is noticeably deeper than the 150 m average shelf depth (i.e., rim depth), reaching 600 m deep at its deepest point (Figure 1b). However, there is a 350 m deep sill at the mouth of the trough which blocks exchange of the deep trough waters with waters offshore (Figure 1b, dashed black line). The sill depth is defined as the deepest isobath connecting the trough to off-shelf waters. The southeastern branch is isolated from the main trunk of the trough by a second 300 m deep sill; whereas the northwestern branch is contiguous with the main trunk until it meets a series of progressively shallower sills (∼200 m deep) at the mouth of Ikersuaq fjord (Bredefjord). Two large marine-terminating glaciers drain into the fjords that open onto Narsaq Trough: Eqalorutsit Kangigdlit Sermiat (two tongues) and Qooroq (Figure 1b, blue and cyan squares); in addition to several smaller marine- and land-terminating glaciers.

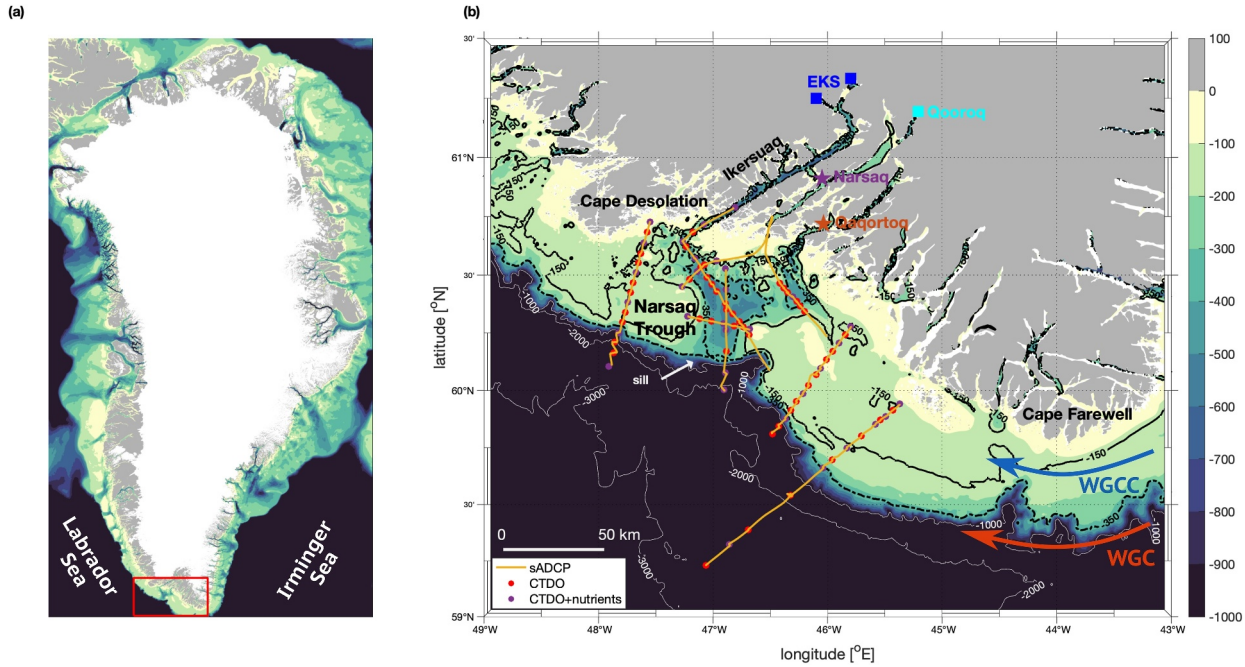

Figure 1. Study region. (a) Bathymetry of the Greenland continental shelf, with the location of Narsaq Trough indicated (red box). (b) Close up of Narsaq Trough bathymetry with observations overlain: sADCP (yellow lines), CTD stations (red circles), and CTD stations with nutrient samples (purple circles). The location of two towns, Qaqortoq (orange star) and Narsaq (purple star), are shown; along with two outlet glaciers, Eqalorutsit Kangigdlit Sermiat (EKS, two tongues; blue squares) and Qooroq (cyan square). Cape Farewell, Cape Desolation, and Ikersuaq fjord are labeled. Isobaths indicating the trough rim depth (−150 m, solid black), sill depth (−350 m, dashed black), and −1,000 m increments (white) are shown. The directions of the West Greenland Current (WGC; red arrow) and West Greenland Coastal Current (WGCC; blue arrow) are marked.

Two currents flowing along the coast in this region are likely to be affected by Narsaq Trough: the West Greenland Current (WGC) and the West Greenland Coastal Current (WGCC) (Figure 1b). The WGC is a coherent full-depth, surface-intensified flow located on the shelf-break that carries warm, salty, oxygen-poor Atlantic Water (AW) (Pacini et al., 2020). The WGCC, on the other hand, is less coherent; at times identifiable as a unique, shallow core on the continental shelf carrying cold, fresh, oxygen-rich Polar Water (PW), at times merged with the WGC, and at times not present at all (Foukal & Pickart, 2023; Gou et al., 2021; Lin et al., 2018). The strength and location of both the WGC and WGCC are influenced by local winds (predominantly upwelling favorable) and remote winds (predominantly downwelling favorable), such that the flow structure is highly variable in time (Foukal & Pickart, 2023; Moore & Renfrew, 2005).

2. Data

2.1. Shipboard Observational Survey

An observational survey of Narsaq Trough was carried out from 5–21 September 2022 on the *R/V Neil Armstrong*. The survey was part of the Overturning in the Subpolar North Atlantic Program (OSNAP) cruise AR69-03, which took place from 19 August to 24 September 2022. 8 transects in and around Narsaq Trough were conducted: 4 cross-shelf transects (far upstream, upstream, midstream, and downstream); 3 cross-trough transects (cross-trunk, northwest branch, southeast branch); and a final transect along the northwestern branch and into the fjord (inner midstream) (Table 1). 82 conductivity-temperature-depth (CTD) stations were occupied over these 8 transects where a SBE911plus system was used to measure temperature and salinity with depth (Figure 1b). An auxiliary SBE 43 oxygen sensor, calibrated with Winklers, was also used. The CTD analysis presented here uses data binned onto 2 dbar pressure levels, except for the Thorpe scale analysis, which uses the 24 Hz data. At 49 stations, discrete water samples were collected for nutrient analysis (nitrate, nitrite, silicate, and phosphate). Ocean current velocities were measured along each transect using a Teledyne RDI 150 kHz Ocean Surveyor shipboard acoustic Doppler current profiler (sADCP). The measured velocities were decided using the Greenland 1 km barotropic tidal model (Gr1kmTM) from Earth and Space Research institute (S. L. Howard & Padman, 2021). High

Table 1
Survey Transect Timing, Number of Stations, Angle of Rotation of Ocean Velocity Coordinates (θ_{rot}), and Mean Along-Shelf Wind Stress During Transect (Positive for Downwelling-Favorable and Negative for Upwelling-Favorable)

Transect[a]	Timeframe (2022, UTC)	# Stations	θ_{rot}[b]	Wind stress $(N.m^{-2})$[c]
(A) Far upstream	22:36 5 Sept–02:37 7 Sept	13	39°	−0.02
(B) Midstream	20:04 7 Sept–05:19 8 Sept	7	87°	−0.03
(C) Cross-trunk	22:08 14 Sept–03:45 15 Sept	6	78°	0.04
(D) Northwest branch	05:03 15 Sept–09:31 15 Sept	5	–	0.13
(E) Southeast branch	20:33 16 Sept–02:03 17 Sept	7	–	0.09
(F) Upstream	16:53 17 Sept–04:42 18 Sept	14	53°	−0.00
(G) Inner midstream	01:05 20 Sept–16:38 20 Sept	15	–	−0.14
(H) Downstream	19:59 20 Sept–12:29 21 Sept	15	74°	−0.36

[a]See Figure S1 in Supporting Information S1 for a map of labeled transects. [b]Angles of rotation for sADCP observations are counter-clockwise from the North-East reference frame. [c]Local winds over the trough during transit occupation (see Text S5, Figure S3 in Supporting Information S1).

resolution bathymetry was measured under the ship-track using the center beam from two shipboard multibeam sonars (Kongsberg EM 122 and EM710). Further details about each of these observational data sets are given in the (Text S1–S4 in Supporting Information S1) along with a map of the transects as labeled in Table 1 (Figure S1 in Supporting Information S1).

2.2. Drifter Trajectories

During the AR69-03 cruise, 12 surface drifters were deployed while on the East Greenland shelf between 60 – 62.3°N, all on the inner-shelf (Figure S2a in Supporting Information S1). The drifters were drogued at 15 m and recorded position hourly. The eight drifters that traveled past Narsaq Trough are used in this study (Figure 2a). The other four drifters ran aground (two prior to rounding Cape Farewell, the third on the islands just upstream of the trough, and the fourth on the coast near the southeast branch of the trough; Figure S2a in Supporting Information S1). Trajectories presented here are unsmoothed. The positional accuracy of the GPS is 2–7 m.

2.3. Bathymetry Maps

For maps presented here, a blended bathymetry product is used which combines BedMachine Greenland (Morlighem et al., 2017) and Etopo1 (Amante & Eakins, 2009; NOAA National Geophysical Data Center, 2009). As BedMachine only extends to the edge of the continental shelf at the southern tip of Greenland, Etopo1 is used to fill in outside of the BedMachine coverage. The resulting product is a 1/200° latitude and longitude grid. The exception is Figure 1a, which uses the original BedMachine product.

3. Methods

3.1. Velocity Rotations

The sADCP velocity sections presented here are rotated into components referenced to the local bathymetry. For the cross-shelf transects (i.e., Figure 3), the velocity is decomposed into along- and cross-shelf components, approximately following the local 1,000 m isobath. Positive along-shelf velocity is toward the northwest (with the mean flow) and positive cross-shelf velocity is onshore. For the cross-trough section (Figure 6e), the velocity is decomposed into in- and cross-trough components, approximately following the local 150 m isobath. Positive in-trough velocity is onshore. The angles of rotation, θ_{rot}, where rotation angles are counter-clockwise from the North-East reference frame, are given in Table 1.

3.2. Section Gridding

The temperature, salinity, oxygen, nutrient, and velocity profile data were gridded along the far upstream, midstream, cross-trunk, and inner-midstream sections (Figures 3, 4, 6 and 7) using the `gridfit` function written

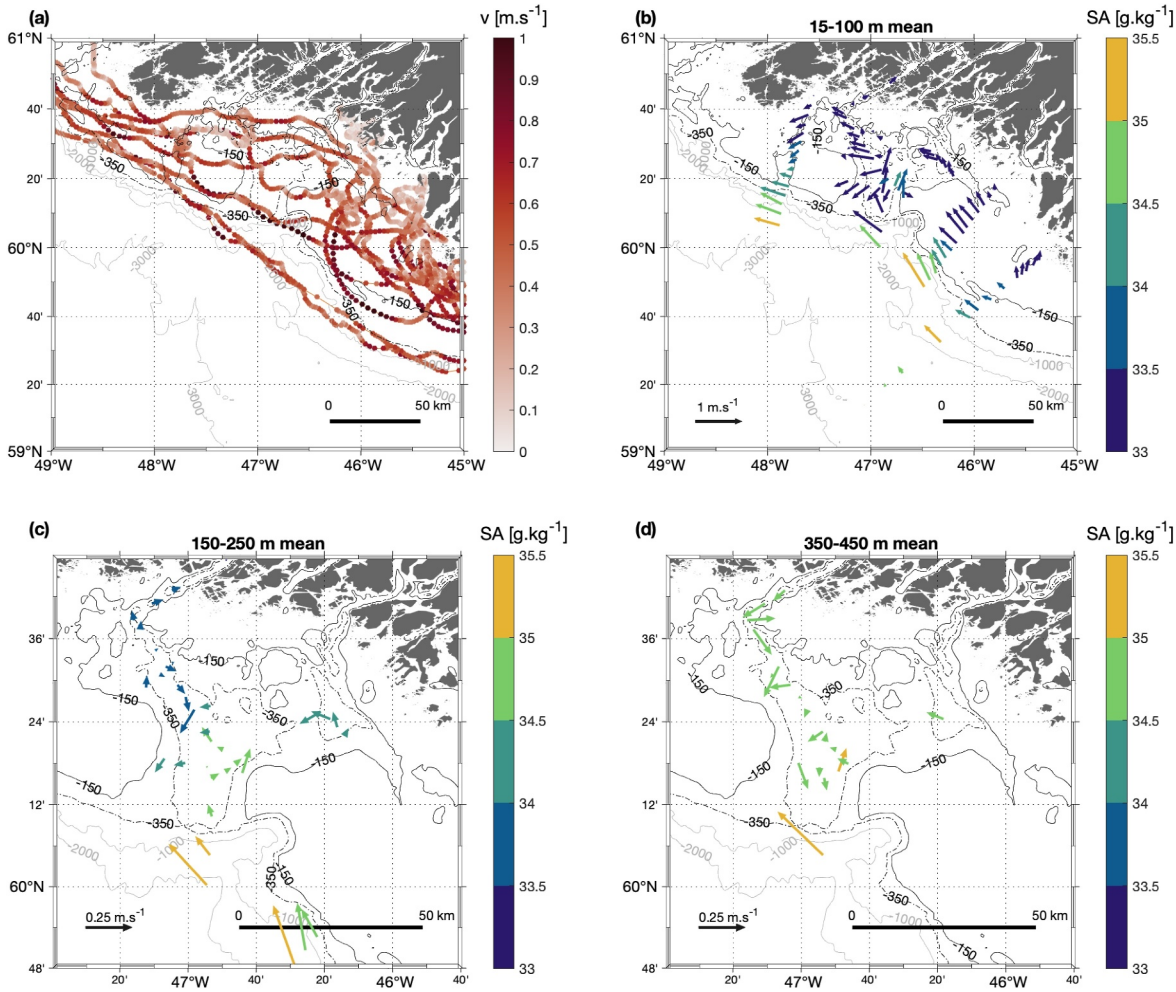

Figure 2. Flow-field at Narsaq Trough. (a) Surface drifter trajectories colored by drifter speed. Depth-averaged velocities in the (b) 15–100 m layer, (c) 150–250 m layer (rim-depth), and (d) 350–450 m layer (below the sill). In panels (b–d) velocity vectors are colored by layer-averaged salinity at the corresponding CTD stations. Note the differing vector scales.

for MATLAB. This gridding interpolates over any data gaps and extrapolates out to the bathymetric boundaries. `gridfit` uses a modified ridge estimator to generate 2D surfaces from scattered data, with a bias toward smoothness (D'Errico, 2006). The triangle interpolation scheme was used, which splits each cell into a triangle and linearly interpolates inside each triangle. For the long transects (far upstream, midstream, downstream, and inner-midstream) a horizontal smoothing scale of 10 and a vertical smoothing scale of 0.5 was used. For the cross-trunk transect a smaller horizontal smoothing scale of 7 (stations are closer together) and a longer vertical smoothing scale of 0.9 (overall range of depths is smaller) were used. The smoothing scales control the tradeoff between data fitting and smoothness of the surface and cannot be converted into meters. The nutrient data were linearly interpolated onto 2 dbar pressure levels prior to gridding to match the vertical resolution of the temperature, salinity, and oxygen data.

3.3. Profile Averaging

To investigate whether unique water properties are found in Narsaq Trough, composite profiles were created to characterize the in-trough, far upstream on-shelf, and far upstream off-shelf environments (Figure 5). The 150 m isobath was used to separate the on- and off-shelf stations along the far upstream transect. The in-trough region composite was made from stations deeper than 350 m inside the main trunk of the trough. For each region, the

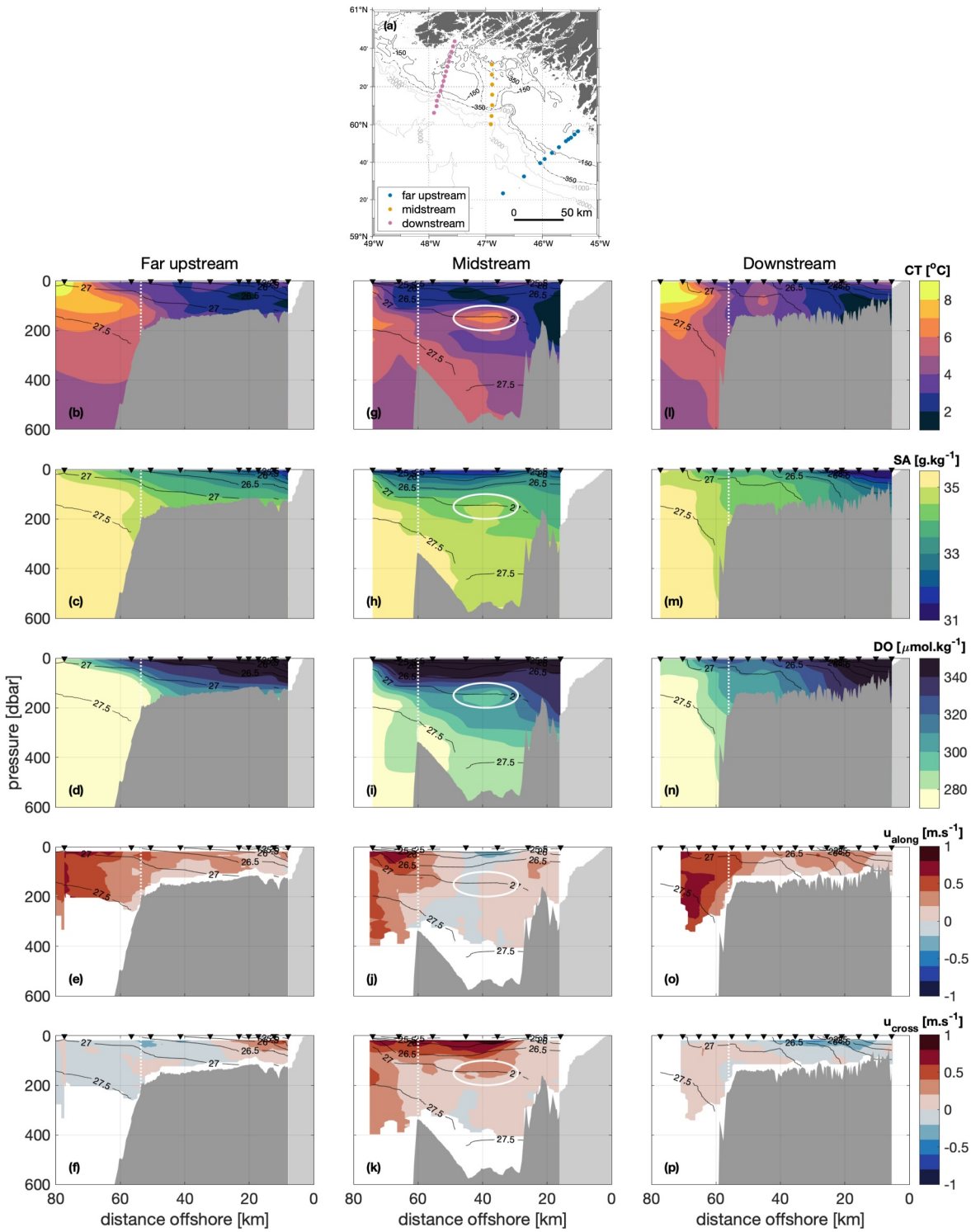

Figure 3. Water properties and flow-field along three cross-shelf transects at Narsaq Trough: (b–f) far upstream, (g–k) midstream (in-trough), and (l–p) downstream; transect locations are shown in panel (a). (b, g, and l) Conservative temperature, (c, h, and m) absolute salinity, (d, i, and n) dissolved oxygen, (e, j, and o) along-shelf velocity (positive to the northwest), and (f, k, and p) cross-shelf velocity (positive onshore). In panels (b–p) isopycnals of potential density (black lines) and CTD stations (black triangles) are overlain. Along-track bathymetry is from the shipboard multibeam sonar (dark gray), extended to the coast using the BedMachine-Etopo product (light gray). The shelf-break is denoted by the white dotted line and an eddy-like feature in the midstream sections is circled in white.

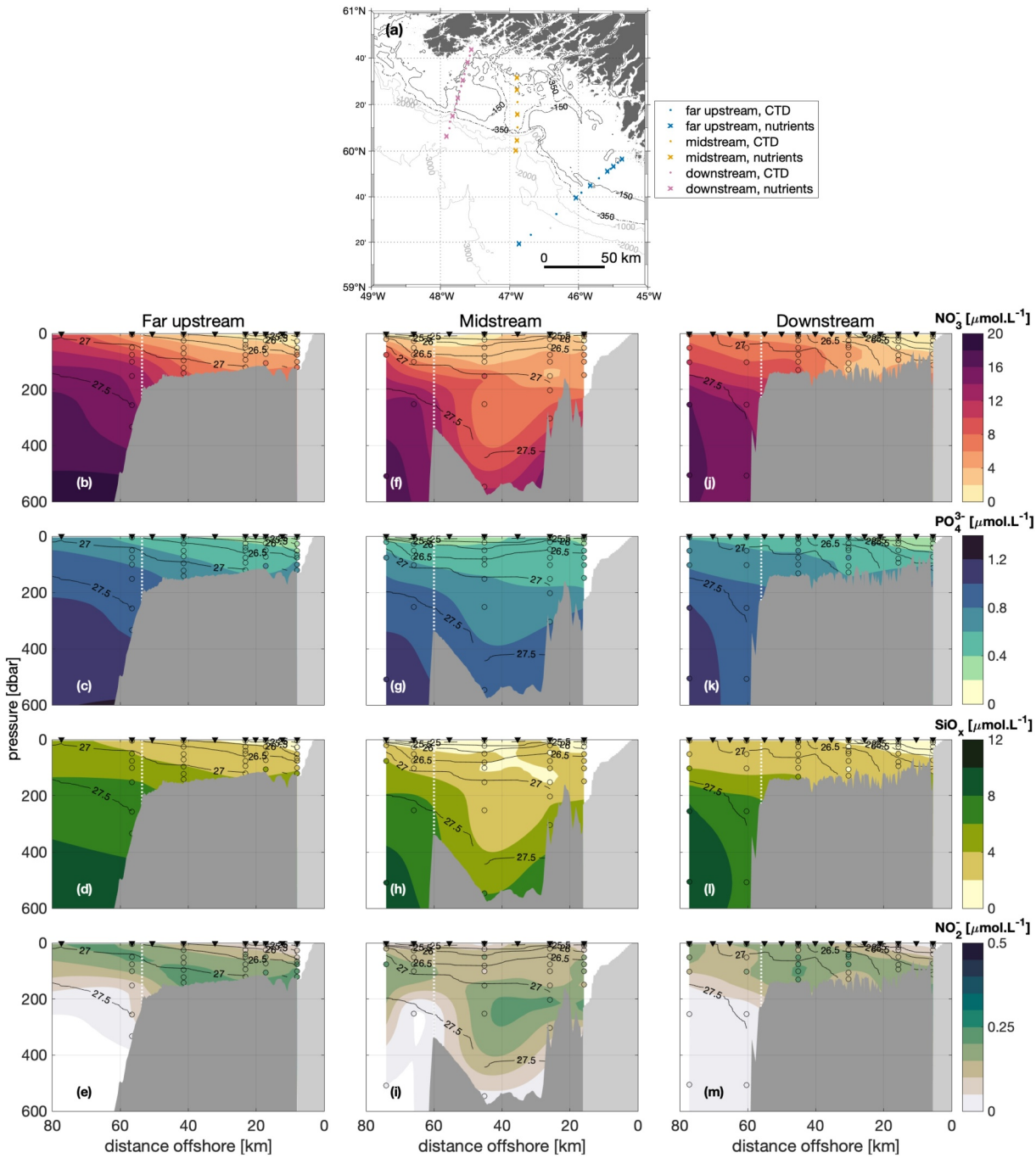

Figure 4. As in Figure 3, but for nutrient concentrations: (b, f, and j) nitrate, (c, g, and k) phosphate, (d, h, and l) silicate, and (e, i, and m) nitrite, with discrete nutrient concentrations used in interpolation overlain (circles). In panel (a) stations with nutrients samples (crosses) are distinguished from those without (dots).

mean and standard deviation of the conservative temperature, absolute salinity, and dissolved oxygen profiles was calculated at each pressure level across all profiles. Data from depths where only one profile exists are excluded.

3.4. Volume, Heat, Freshwater and Oxygen Transports

The volume, heat, freshwater and oxygen exchanges across the trough's trunk were estimated by calculating the inflow and outflow at the cross-trunk transect, between the trough rim and sill (i.e., 150–350 m; Table 2, see Figure 6 for transect location). Transports were calculated using the gridded temperature, salinity, oxygen and in-

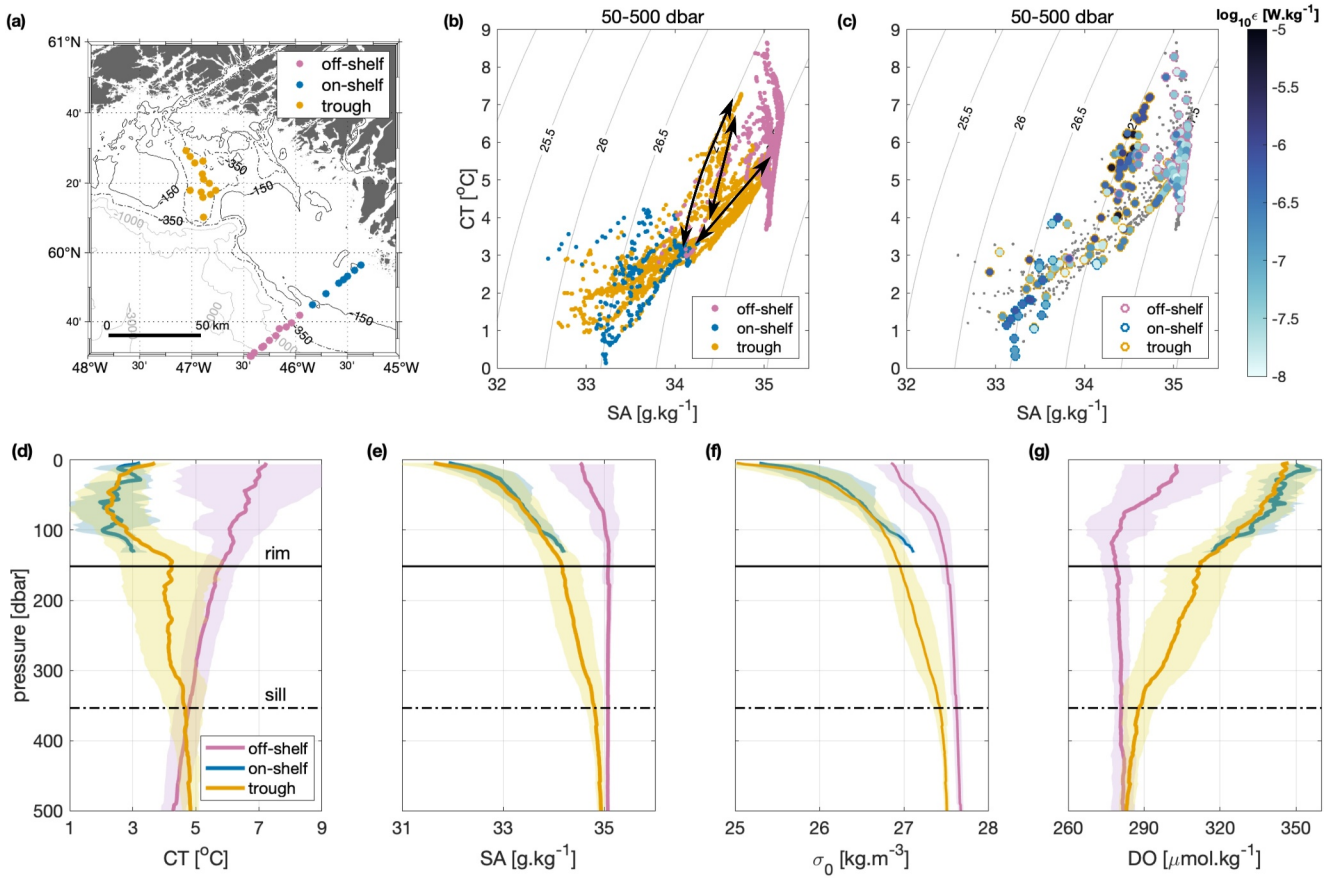

Figure 5. Comparison of water properties far upstream to inside the trough. (a) Map showing stations used in regional averages and subsequent panels; off-shelf (pink), on-shelf (blue), trough (orange). (b) T-S diagram comparing water properties by regions for the 50–500 dbar layer. (c) T-S diagram of all points in panel (b) colored by dissipation rate for points with $\epsilon > 10^{-8}$ W.kg^{-1}. Mean (d) conservative temperature, (e) absolute salinity, (f) potential density and (g) dissolved oxygen profiles; shading shows one standard deviation about the mean. Black arrows in panel (b) indicate mixing pathways.

trough velocity fields. The zero-crossing of the depth-integrated velocity over the sill-to-rim layer was used to divide the inflow from the outflow, which was found to be at $x_0 = 15.9$ km. Transport fields were then vertically integrated over the sill-to-rim layer and horizontally integrated over the inflow ($x1 = 0, x2 = x_0$ km) and outflow ($x1 = x_0, x2 = 30$ km). Volume transport is thus calculated as

$$\text{Volume transport} = \int_{x1}^{x2} \int_{-350}^{-150} u_{\text{in-trough}}(x,z)\, dz\, dx, \tag{1}$$

where $u_{\text{in - trough}}(x,z)$ is the gridded in-trough velocity field. Heat transport is calculated as

$$\text{Heat transport} = \rho_0 c_p \int_{x1}^{x2} \int_{-350}^{-150} u_{\text{in-trough}}(x,z)\, T(x,z)\, dz\, dx, \tag{2}$$

where $\rho_0 = 1027$ kg.m^{-3}, $c_p = 3850$ J.kg^{-1} .K^{-1}, and $T(x,z)$ is the gridded conservative temperature field in Kelvin. Freshwater transport is calculated with respect to a reference salinity of $S_{\text{ref}} = 35.1$ g.kg^{-1} (which is the depth-averaged salinity over the 150–350 m layer of the far upstream composite profile, see Section 3.3),

$$\text{Freshwater transport} = \int_{x1}^{x2} \int_{-350}^{-150} u_{\text{in-trough}}(x,z) \frac{S_{\text{ref}} - S(x,z)}{S(x,z)}\, dz\, dx, \tag{3}$$

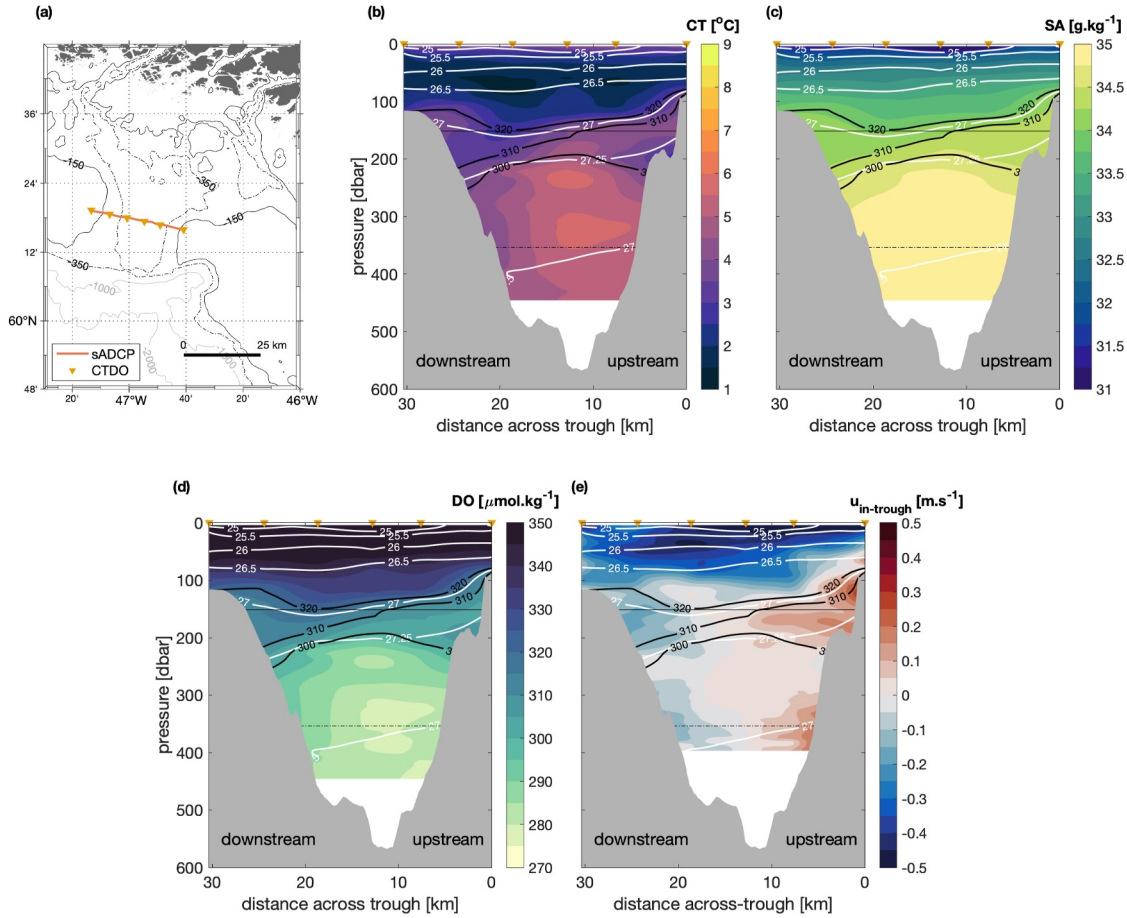

Figure 6. Cross-trough transect sections. (a) Map showing location of sADCP transect (orange line) and CTD stations (orange triangles). Cross-trough (b) conservative temperature, (c) absolute salinity, (d) dissolved oxygen, and (e) in-trough velocity (positive toward the coast) fields. In panels (b–e) isopycnals (white lines), rim depth (150 m, black line), sill depth (350 m, black dashed line), CTD stations (orange triangles), and the 300, 310, and 320 μ mol.kg^{-1} oxygen contours (thick black lines) are overlain. Bathymetry in panels (b–e) is from the shipboard multibeam sonar.

where $S(x,z)$ is the gridded absolute salinity field in g.kg^{-1}. Finally, the oxygen transport is calculated as

$$\text{Oxygen transport} = \rho_0 \int_{x1}^{x2} \int_{-350}^{-150} u_{\text{in-trough}}(x,z)\, DO(x,z)\, dz\, dx, \tag{4}$$

where $DO(x,z)$ is the gridded dissolved oxygen field in μ mol.kg^{-1}.

3.5. Mixing Analysis

3.5.1. Estimating Turbulent Dissipation Rate and Vertical Diffusivity

To quantify turbulent fluxes of heat or other tracers across isopycnals in the vicinity of the trough, an estimate of the turbulent mixing is needed. This can be estimated through the turbulent dissipation rate, ϵ, the key variable that drives overturning and mixing in a stratified water column (Osborn, 1978). Here, we estimate ϵ from vertical density overturns using estimates of the Thorpe scale, L_T (Galbraith & Kelley, 1996; Thorpe, 1997), and the Ozmidov scale, L_O (Ozmidov, 1965):

$$\epsilon = (cL_T)^2 N^3, \tag{5}$$

where $c = L_O/L_T = 0.8$ (Dillon, 1982) and N is the buoyancy frequency.

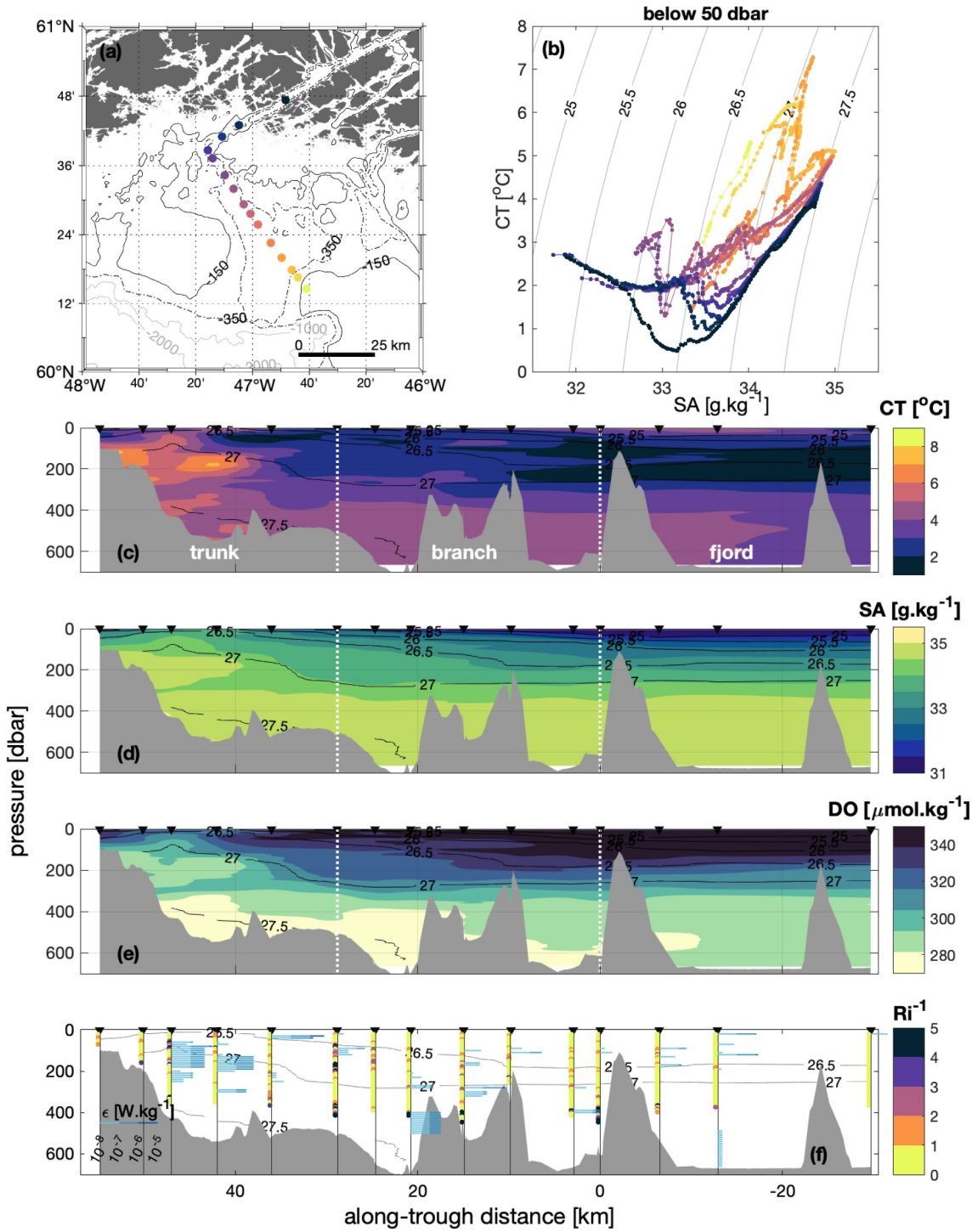

Figure 7. Inner-midstream transect entering Ikersuaq fjord. (a) Map of CTD stations, colored by location. (b) T-S diagram, colored by location as in panel (a). (c–e) As in Figure 3, but for the inner-midstream transect; dashed white lines indicate the CTD stations used to delineate the trunk of the trough, northwest branch, and fjord. (f) Estimated dissipation rates (ϵ, blue bars) with inverse Richardson number estimates (Ri^{-1}, colored dots) overlain.

We quantify the turbulent dissipation rate using the 24 Hz CTD data. These data were corrected for the lag between the temperature and conductivity cell, pressure and temperature were despiked and delooped, and finally salinity was despiked. Following Fer et al. (2004), each observed potential density profile was used to create an artificial density profile by re-ordering it to be gravitationally stable. Then, we estimate the vertical displacements

Table 2
Column-Integrated Volume, Heat, Freshwater, and Oxygen Transport in the 150–350 m Layer (Between the Trough Rim and Sill) as Calculated From the Cross-Trunk Transect

	Inflow	Outflow
Volume transport [mSv]	97	96
Heat transport [PW]	0.106	0.105
Fresh water transport [mSv]	1.3	1.8
Oxygen transport ($\times 10^4$ mol.s^{-1})	2.95	2.99

needed to move fluid parcels from their depths in the observed profile to the reordered profile, within the depth span of a given overturn. The Thorpe scale is defined as the root-mean-square of all non-zero displacements. We use a minimum run length criteria of 6 m (Fer et al., 2004) and a minimum overturn size of 2 m to distinguish overturns from noise and error. The orders of magnitude of the ϵ estimates presented here are not sensitive to changes in the run length and overturn size criteria between 1 and 10 m. Finally, the ϵ estimates are averaged over 10 m bins (Figures 5c and 7f). Note that during the cross-trough transect (Figure 6) the CTD heave due to the ship motion was too big to make reliable estimates of dissipation using this method.

The vertical diffusivity in the trough, κ_z, can then be estimated from ϵ following Osborn (1980): $\kappa_z = \gamma\epsilon/N^2$, where γ is the mixing efficiency and we assume $\gamma = 0.2$.

3.5.2. Advection-Diffusion Model

A simplified advection-diffusion model, described by Voet et al. (2015), is used to provide an upper bound estimate of the local vertical dissipation needed to create the observed sub-surface cross-trough salinity and oxygen gradient. While this advection-diffusion model does not include the effects of convergences of meltwater with the oceanic water, it provides an order of magnitude estimate of one of the mechanisms resulting in the observed gradients in the trough. The model estimates the magnitude of vertical diffusivity needed to modify the inflowing waters to match the outflow properties. Briefly, following Hautala et al. (1996), the vertical mixing of tracer concentration C can be modeled as

$$\frac{DC}{Dt} = \kappa_z \frac{\partial C}{\partial z}. \tag{6}$$

The observed change in the tracer is dependent on κ_z and the time scale, t_c, over which the change occurs. These two parameters can be combined into a vertical spreading scale, $\lambda = \left(\kappa_z t_c\right)^{1/2}$. Here, we apply the advection-diffusion model to the T-S profile in the core of the inflow in the cross-trunk section (Figure 6, second profile from the right) and determine the vertical spreading scale needed to match the T-S properties of the core of the outflow (Figure 6, fourth profile from the left). The tracer concentrations (T and S in this case) are held constant at 100 m and a no flux boundary condition is imposed at the bottom.

4. Results

Below we describe findings from the observational survey. First, we describe how the flow-field and water mass distribution over the continental shelf differs at the trough compared to up- and down-stream. Second, we show that the trough creates a unique in-trough environment that supports a sub-surface circulation. Third, we present estimates of the turbulent dissipation rate and diffusivity to evaluate the water mass transformation and mixing occurring in the trough.

4.1. Cross-Shelf Structure of Flow-Field and Water Mass Distribution

The flow-field at Narsaq Trough was observed to have a different structure than upstream or downstream of the trough, with no clear WGCC core over the trough and with notable cross-shelf flow in and over the trough (Figures 2 and 3). For this analysis, we define the WGC as the velocity core located at or off the shelf-break, with salinities greater than 34 g.kg^{-1} (Foukal & Pickart, 2023; Pacini et al., 2020). The WGCC is identified as a separate core if there is a velocity peak inshore of the WGC core, typically with salinities less than 33 g.kg^{-1} (Foukal & Pickart, 2023).

At the surface, there are two main pathways for flow passing the trough: the trough deflects the WGCC onshore while the WGC continues to follow the shelf-break (Figures 2a and 2b). The salty WGC core follows the large-scale bathymetry of the shelf-break at all cross-shelf transects, although the width of the current varies and is not always fully captured. Whereas the fresher WGCC is directed toward the coast upstream and back out toward the

shelf-break downstream. While a clear WGCC core was not observed at the midstream transect it may have been located in the gap between the end of the transect and the coast. In sum, these observations are illustrative of the WGCC following isobaths and being deflected around the head of the trough.

Surface drifter trajectories past the trough in August–October 2022 are consistent with the two identified pathways (Figure 2a). Each drifter took 2–7 days to cross the trough (from −46°E to −48°E), except one which took 15 days (Figure S2b in Supporting Information S1). Drifters in the WGC (between the 150 and 2,000 m isobath) upstream of the trough have relatively fast, well-organized trajectories and follow the shelf-break past the trough undeflected. On the other hand, drifters on the shelf have slow, eddying, poorly-organized trajectories upstream of the trough and are mostly deflected around the head of the trough. The drifters on the shelf emerge downstream of the trough in a more coherent, faster WGCC pathway. One drifter passed slowly over the trunk of the trough, while two drifters that start on the shelf exit the shelf and join the WGC while passing the trough.

Consistent with past studies, upstream of the trough the continental shelf separates the warm, salty, oxygen-poor Atlantic Water (AW) in the WGC (peak along-shelf velocity of 0.6 $m.s^{-1}$, 75 km offshore) from the cold, fresh, oxygen-rich Polar Water (PW) in the WGCC (Figures 3b–3e; peak along-shelf velocity of 0.3 $m.s^{-1}$, 25 km offshore). There is very little cross-shelf velocity far upstream, consistent with weak wind forcing during the transect (Figures 3f and Table 1). In contrast, at the trough, AW is observed inshore of the shelf-break, under the PW (Figures 3g–3i), consistent with strong onshore cross-shelf velocity at the mouth of the trough (Figures 3k, 0–400 m deep, 60–75 km offshore). The onshore velocity cannot simply be explained by the local wind forcing during the transect (weak winds; Table 1). The WGC core remains intact past the trough mouth (Figure 3j; peak along-shelf velocity of 0.4 $m.s^{-1}$, 75 km offshore, with a stronger surface core peaking at 0.7 $m.s^{-1}$, 65 km offshore), whereas there is no evidence of the WGCC passing over the trough. Additionally, an eddy-like pulse of AW was observed 20 km inshore of the shelf-break at the depth of the rim of the trough (Figures 3g–3i, circled in white), discussed further in Section 5.1.

The cross-shelf distribution of nutrients in the trough is also notably different than far upstream (Figure 4). Far upstream, the on-shelf waters are depleted in macro-nutrients (nitrate, phosphate, and silicate), whereas off-shelf macro-nutrient concentrations are higher in the surface waters and increase further with depth (Figures 4b–4d). Over the trough, low macro-nutrient surface waters extend past the shelf-break and waters below the shelf depth are depleted in nutrients relative to waters at the same depth off-shelf (Figures 4f–4h). Nitrite concentrations are high in the upper 200 m both on- and off-shelf far upstream, with no nitrite at depth (Figure 4e). In the trough, however, high nitrite waters are only found below 200 m (Figure 4i).

Downstream of the trough properties and velocities generally resemble the upstream distribution, with several relevant changes: Firstly, a warm anomaly is observed inshore of the shelf-break (5°C, 45 km offshore; Figure 3l). Secondly, the PW is more tightly banked up against the coast, driving a more coherent WGCC (Figures 3l–3o). Thirdly, waters above the sill depth, offshore of the shelf-break, are lighter, fresher, and more oxygen-rich downstream than far upstream (Figures 3m and 3o; 150–350 m, 60–70 km offshore). Finally, waters with lower macro-nutrient concentrations are found on the continental slope downstream (Figures 4j–4l; 400–600 m, 60–70 km offshore), where there are none upstream (Figures 4b–4d). These differences cannot be explained by the upwelling winds during the transect.

4.2. Unique In-Trough Environment

By comparing composite profiles of waters in and upstream of Narsaq Trough the differences in water properties are evident. Far upstream, the off-shelf waters have typical AW properties: warm, salty, dense, and oxygen-poor (Figures 5d–5g, pink); and the on-shelf waters have typical PW properties: cold, fresh, light, oxygen-rich (Figures 5d–5g, blue). At the trough, waters above the rim of the trough have properties that are indistinguishable from the on-shelf waters far upstream; while waters below the rim of the trough are fresher, lighter, more oxygen-rich, and, at times, colder than the off-shelf waters far upstream (Figures 5d–5g, orange). These differences are largest between the rim and sill depth (150–350 m). The unique in-trough waters appear to be a mixture of AW and PW, spanning the gap between AW and PW in T-S space. Specifically, the distribution of points in T-S space is suggestive of mixing occurring both along (27 $kg.m^{-3}$) and across (between 27 and 27.5 $kg.m^{-3}$) isopycnals (Figure 5b). This mixing is analyzed in Section 4.3.

Below the sill depth, waters in the trough are on average warmer than waters at the same depth off-shelf (Figure 5d), consistent with the sill setting the depth of exchange between deep waters in the trough and off-shelf waters. As such, we expect the water properties below the sill depth in the trough to have similar properties at sill depth off-shelf. Additionally, a small vertical property gradient below the sill depth is observed in the trough profiles (Figures 5d–5g), indicative of vertical mixing between the overlying layer and the deep waters trapped in the trough. This mixing could be explained by turbulence as waters spill over the sill (Venables et al., 2017) and velocity-shear from the secondary circulation at sill depth (Figure 6e).

Further, cross-trough asymmetry in sub-surface waters was observed in the trough, 18 km inshore of the mouth. A salty, oxygen-poor inflow on the upstream wall of the trough and a fresher, oxygen-enriched outflow on the downstream wall supports a cyclonic circulation between 150 and 250 m (Figures 2c and 6). Specifically, inflowing waters have oxygen concentrations of between 300 and 310 μ mol.kg^{-1}, compared to concentrations of 310–320 μ mol.kg^{-1} in the outflowing waters (Figures 6d and 6e). While a similar cross-trough gradient is seen in salinity, the asymmetry is not as evident in temperature as the system is salinity-stratified with considerable temperature interleaving (Figures 6b and 6c). Even at depth in the trough, below the depth of the sill (350–450 m), a cyclonic circulation supports a small cross-trough salinity gradient (Figures 2d and 6e), which is striking given the sill blocks free exchange with off-shelf waters.

The sub-surface cyclonic circulation can be described as a horizontal exchange flow, with a volume transport of 97 mSv, symmetric about the axis of the trough (Table 2, Figure 6). Despite the symmetric volume transport, the cross-trough gradient in salinity and oxygen results in greater freshwater and oxygen transports out of the trough than in; indicative of AW mixing with PW in the trough (Table 2, Figure 6). The residence time for waters in the trough between the rim and sill is given by $t_R = \frac{Vol}{T_{ex}}$. Vol is the volume of interest within the trough, assumed to be the area of the main trunk of the trough over the 150–350 m layer, such that $Vol = 2.4 \times 10^{11}$ m^3. Using the exchange flow as the volume transport, T_{ex}, the residence time for waters between the rim and sill is estimated to be 30 days.

The unique in-trough environment is connected to Ikersuaq fjord via the northwest branch of Narsaq Trough. In general, surface waters become colder, fresher, and more oxygen-rich toward the fjord, although surface waters in the fjord are warmer than in the northwest branch (Figures 7c–7e, 0–100 dbar). A similar general signal is seen at mid-depth, with a stronger horizontal gradient in water properties between the trunk of the trough and the northwest branch than between the northwest branch and the fjord (Figures 7c–7e, 150–350 dbar). This is in part due to the pocket of warm, salty, oxygen-poor water on the upstream wall, associated with inflowing waters from the shelf-break (Figures 7c–7e, x > 40 km). Below 350 dbar, AW was observed along the length of the northwest branch and inside the fjord with little horizontal gradient in water properties. We note, however, that the transect track does not trace the expected pathway of waters entering the northwest branch. The trough-fjord connectivity is discussed in Section 5.2.

4.3. Estimates of Turbulent Dissipation Rate and Diapycnal Mixing

Using the Thorpe scale analysis described in Section 3.5.1, we find that turbulent dissipation rates, ϵ (and subsequently diffusivities, κ_z), are elevated in the trough (Figures 5c and 7f). Notably, ϵ values of up to 10^{-5} W.kg^{-1} are observed in the trough, which is three orders of magnitude higher than in an Antarctic trough (Scott et al., 2021) and two orders of magnitude higher than on the continental shelf in Svalbard (Fer, 2006) or mixing hot spots on the United States continental slope (Nash et al., 2007). Dissipation rates upstream of the trough are also high (10^{-6} W.kg^{-1}; Figure 5c). In particular, elevated dissipation is seen where pockets of warm, salty, oxygen-rich AW exist in the trough, likely mixing the AW with PW (e.g., Figure 7 at 100–300 m depth, 40–50 km along-trough). We note that high ϵ values are also observed at depth in the trough near steep topography, but there is no PW at this depth to create the modified-AW. Estimating the vertical diffusivity in the trough over the 150–350 dbar layer using $\kappa_z = \gamma\epsilon/N^2$ (Section 3.5.1), we find $10^{-5} < \kappa_z < 10^{-1}$ m^2.s^{-1}, with $\overline{\kappa_z} = 10^{-3}$ m^2.s^{-1}. This mean diffusivity is an order of magnitude higher than typically reported for Antarctic troughs (Klinck, 1998; diffusivity estimated from a semi-spectral primitive equation model), or in Arctic fjords and on the Greenland shelf (Bendtsen et al., 2021; Fer, 2006; diffusivities estimated from microstructure measurements).

One way for vertical dissipation to be enhanced is through shear-driven mixing which can be identified using the Richardson number. The Richardson number is defined as $\mathrm{Ri} = \frac{N^2}{Sh^2}$, where Sh is the vertical shear in the two-

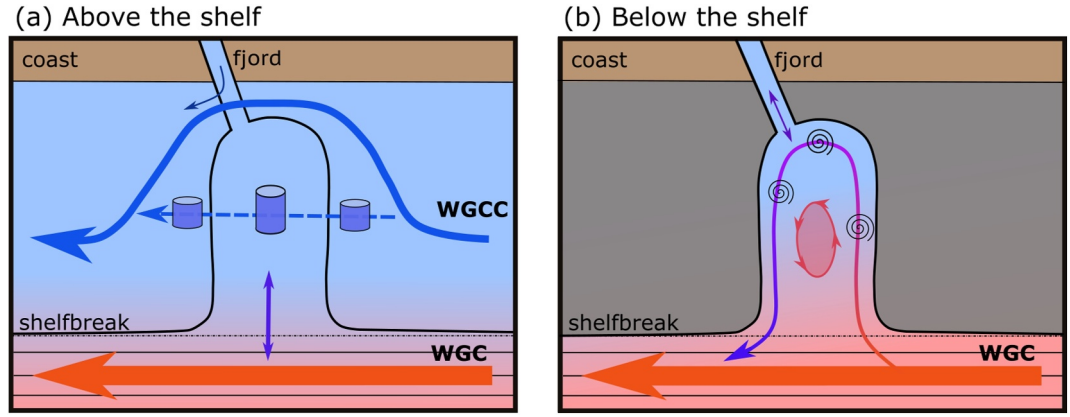

Figure 8. Schematic illustrating flow-field, cross-shelf exchange mechanisms, and modification of AW (a) above the shelf (0–150 m) and (b) below the shelf, between the trough rim and sill (150–350 m). Blue shading indicates PW, red shading indicates AW. Arrows show the two main currents (WGC, red; WGCC, blue), surface flow reversals over the trough ((a) purple), fjord outflow ((a) dark blue), exchange flow ((b) red-to-purple), sub-surface fjord exchange ((b) purple), and an eddy ((b) pink). In panel (a) cylinders represent vortex tubes and in panel (b) spirals indicate mixing and modification of AW.

dimensional velocity field (L. Howard, 1961; Miles, 1961). Typically, vertical velocity shear is deemed strong enough to overcome vertical stratification and drive mixing at Ri < 1/4, however, due to the 8 m resolution of the sADCP data, we use a more relaxed threshold of Ri < 1 ($Ri^{-1} > 1$) (MacKinnon et al., 2021). In several sections, sub-critical Ri values are observed between 100 and 200 dbar, that is, at the rim depth (e.g., Figure 7f), co-located with where the surface PW meets the subsurface AW circulation (Figure 6). This indicates that the mixing creating the modified AW in the trough is due, at least in part, to shear-driven instabilities.

To assess whether it is possible for the sub-surface cross-trough salinity and oxygen gradient to be created through turbulent vertical mixing processes within the trough, rather than variability in the properties of the inflowing water, we use a simple advection-diffusion model (Section 3.5.2). A vertical spreading scale of $\lambda = 150$ m is found to be sufficient to modify the inflow properties to the match outflow properties. Taking t_c as the 30 days residence time calculated in Section 4.2, the vertical diffusivity needed to drive this modification is estimated to be 10^{-2} $m^2 .s^{-1}$. While this κ_z is within the range of values measured in the trough, it is above the mean ($\overline{\kappa_z} = 10^{-3}$ $m^2 .s^{-1}$), such that advection may play a role. Additionally, we note that any cold, fresh, oxygen-rich sub-surface waters exiting the fjord may contribute additional source water to the modified layer, reducing the vertical mixing needed as estimated using this model. However, we expect the submarine meltwater (or meteoric water) transport to the shelf from local glaciers will be orders of magnitude smaller than the transport of the WGCC (<5 mSv, Beaird et al., 2023; versus ~800 mSv, Foukal & Pickart, 2023).

5. Discussion

5.1. Cross-Shelf Exchange and Water Mass Modification

Transport of AW into Narsaq Trough is likely due to bathymetric steering of mean flow and eddies—indications of which were observed during the survey and which are illustrated in Figure 8. We propose that AW transported into the trough is then mixed with the overlying PW and any water escaping the fjord below the surface, primarily through shear-driven mixing and likely supported by trough-induced downwelling and vortex stretching. These processes are discussed below.

The exchange flow in the trunk of the trough (Figure 6e) can be characterized as a bathymetrically-steered leakage from the WGC (Figure 8b). Based on canyon theory, we expect that when the leakage is steered into the trough along the upstream wall it is downwelled, with upwelling occurring on the downstream wall (Freeland & Denman, 1982; Klinck, 1996). Klinck (1996) suggested that when dissipation is strong, as is the case here (Figures 5c and 7f), upwelling on the downstream wall is reduced (assuming diapycnal mixing), resulting in net downwelling in the trough.

A low Rossby number, *Ro*, indicates that sub-surface flow is likely to follow isobaths and circulate around the canyon (Allen & Hickey, 2010; Spurgin & Allen, 2014). The *Ro* is defined as $Ro = U/fr$, where U is the upstream flow speed at the depth of the trough rim, f is the Coriolis frequency, and r is the radius of curvature of the upstream isobaths as they bend into the trough (Allen & Hickey, 2010). For Narsaq Trough, *Ro* is estimated to be 0.12 ($U = 0.3$ m.s^{-1}, Figure 3e, at 150 m depth, 60 km offshore; $r = 20$ km following the large-scale bathymetry), which is low ($Ro < 0.2$, Spurgin & Allen, 2014). The sub-surface circulation observed at Narsaq Trough (Figure 6e) is therefore consistent with theory. Since the strength and location of the WGC core is variable (Foukal & Pickart, 2023), the flow upstream of the trough may at times be too fast to follow isobaths, such that the exchange flow within the trough is likely episodic. Further, the bathymetry just upstream of the trough makes a sharp bend, which exacerbates the likelihood that flow will separate from the bathymetry.

The warm, salty, oxygen-rich pulse of water observed at the head of the trough has the appearance of an eddy (Figures 3g–3i, circled in white; illustrated in Figure 8b). These anomalous water properties are co-located with a reversal in the along-shelf velocity, further supporting the eddy hypothesis (Figure 3j). Based on the along-shelf velocity, the eddy-like feature can be characterized as cyclonic, with a radius of 5 km. Studies in Antarctica have shown that eddies preferentially cross the shelf-break at troughs and account for up to 50% of on-shelf heat transport at troughs (Couto et al., 2017; Martinson & McKee, 2012). As such, eddies entering troughs are likely also a major source of heat and AW to the Greenland shelf. These eddies could be generated by Rossby waves propagating along the shelf-break (St-Laurent et al., 2013).

Once the AW is advected on-shelf, either by bathymetric steering of the mean flow or by eddies, it is proposed that the AW is modified by shear-driven mixing in the trough (Figure 8b). Strong vertical shear in the velocity field is observed in the trough, in part due to a reversal of the surface flow between the two transects (Figures 6e and 7f, 100–200 m, and illustrated in Figure 8b). The high shear is co-located with depths of high dissipation (Figure 7f), suggesting velocity shear is likely driving vertical fluxes. Brearley et al. (2017) show that velocity shear resulting from wind-driven currents is a key source of vertical mixing between overlying water masses on the Antarctic Peninsula, however, the surface flow reversal observed here cannot easily be explained by local wind forcing as the local wind forcing was weak during both transects (Table 1, Figure S3 in Supporting Information S1). In addition to shear-driven mixing, any PW not able to follow isobaths upon encountering the trough will experience vortex stretching as water parcels transit into deeper water, bringing PW into contact with AW and supporting mixing (Figure 8a).

While we have presented some evidence of trough modified waters exported downstream (Section 4.1, Figures 3 and 4), we cannot rule out that some of the upstream/downstream differences are due to WGC variability (Foukal & Pickart, 2023). A comparison of freshwater and oxygen transport differences from upstream to downstream did not lead to conclusive results, which we attribute, in part, to differing wind conditions (weak vs. strong upwelling; Table 1; Figure S3 in Supporting Information S1). Understanding the impact of Greenland's troughs to transporting the freshwater and oxygen offshore will require further studies that can estimate long-term means (Hendry et al., 2021; Luo et al., 2016; Schiller-Weiss et al., 2024).

5.2. Implications for Fjords and Marine-Terminating Glaciers

Previous studies in Antarctica have shown that troughs drive an onshore heat flux, contributing to the melting of ice shelves (Couto et al., 2017; Moffat & Meredith, 2018; Silvano et al., 2022). Here we show that AW is modified in the trough (Figure 5), such that any AW that makes it into the adjoining Ikersuaq fjord is colder than unmodified AW (and has higher oxygen), consistent with Klinck (1998). The deepest isobath connecting the fjord and trough sets the level at which waters can be freely exchanged between the two. For Narsaq Trough and Ikersuaq fjord, existing estimates of this depth vary: 185 m (BedMachine, Morlighem et al., 2017), 330 m (Mortensen et al., 2020), 200–400 m (Nørgaard-Pedersen & Mikkelsen, 2009), or more than 400 m (Ribergaard, 2007). Our multibeam survey showed a series of sills, reaching 100 m at the shallowest point (Figures 7c–7f), but we could not determine the deepest connected isobath from our survey. However, the water properties inside the trough and fjord between the 150–350 dbar are very similar (Figure 7 and Figure S4 in Supporting Information S1), consistent with a deep connection. It is likely that additional mixing occurs as waters spill over the series of sills into the fjord, which will further reduce the temperature of the water mass where the sills are shallow enough to drive mixing between PW and AW (Venables et al., 2017).

5.3. Implications for Biological Productivity

The Greenland continental shelves are known to be biologically productive, especially in the south (Krawczyk et al., 2021; Vernet et al., 2021), but the effect of troughs on this productivity has not been studied. In the summer, productivity on the shelf is thought to be nitrate-limited (Hopwood et al., 2018), which would be alleviated if troughs delivered nutrient-rich water to the euphotic zone. However, Narsaq Trough likely supports net downwelling and elevated nutrient concentrations are not seen over the trough.

Observations in Narsaq Trough do, however, show that macronutrients are depleted at depth, relative to waters at the same depth off-shelf and far upstream (Figures 4b–4d, and 4g–4i). These observations are consistent with the dynamical explanation that vertical mixing, likely through velocity shear and supported by downwelling and vortex stretching, results in exchange between the nutrient-poor PW and nutrient-rich AW. The absence of a signal of nutrients mixed up into the surface waters can be explained by the rapid replenishment of surface waters over the trough, whereas waters in the trough have a longer residence time, allowing for depletion/dilution.

We note that our observations of lower sub-surface nutrient concentrations in the trough than off-shelf differ from previous findings in Greenland. Hendry et al. (2019) show elevated sub-surface nutrient concentrations in Nuuk Trough compared with off-shelf, which they attribute to contributions from glacial discharge. Their observations were taken at a similar time of year (July–Aug, 2017), suggesting that the difference is not due to seasonal variability. One difference of note is that Nuuk Trough has a shallow retrograde slope along the length of the trough, whereas Narsaq Trough has a steep retrograde slope at the mouth before leveling out and rising again toward the head. The steeper sill at Narsaq Trough may be more conducive to driving mixing between AW and the overlying, nutrient-poor PW, thus reducing sub-surface nutrient concentrations.

6. Conclusions

Narsaq Trough, in southwest Greenland, is found to provide a pathway for AW to intrude onto the continental shelf where these waters are mixed with the overlying PW. As a result, sub-surface waters in the trough are fresher, oxygen-enriched, macronutrient-depleted, and at times colder, relative to the unmodified AW offshore. For the AW that is transported into the connected fjord, mixing within the trough reduces the heat content of the waters that can access the outlet glaciers in Ikersuaq fjord. Additionally, the cyclonic circulation in the trough may export the modified AW back out onto the shelf-break and into the WGC. Export of the trough-modified waters could act to cool, freshen, and oxygenate the WGC, potentially increasing stratification and decreasing deep water formation in the adjacent convective basin. While there is a substantial body of literature documenting troughs driving heat and salt import onto continental shelves, particularly in Antarctica, few studies have considered the degree to which troughs modify inflowing water or drive export of shelf waters (although Brearley et al., 2019; Venables et al., 2017 are two notable examples). As such, this work provides novel insights about the role of troughs in Greenland and shows that considering the cumulative effects of the numerous troughs around Greenland's margin warrants further investigation.

Data Availability Statement

The temperature and salinity profile data and the nutrient bottle data are available at CCHDO via https://cchdo.ucsd.edu/cruise/33VB20220819 (Straneo, 2023). This includes both the 24 Hz data and the 2 dbar binned data. The bottle-calibrated oxygen profile data are available at BCO-DMO via https://www.bco-dmo.org/dataset/933743 (Fogaren & Palevsky, 2024). The ocean velocity data are available at Rolling Deck to Repository via https://doi.org/10.7284/153091 (Straneo, 2022a). Along-track bathymetry used in the sections presented here are available at Rolling Deck to Repository via https://doi.org/10.7284/153098 and https://doi.org/10.7284/153099 (Straneo, 2022b, 2022c). The drifter trajectories are available through the NOAA Global Drifter Program repository via https://www.ncei.noaa.gov/access/metadata/landing-page/bin/iso?id=gov.noaa.nodc:AOML-GDP-1hr (Elipot et al., 2022). The BedMachine bathymetry data used to make the maps presented here are available at the National Snow and Ice Data Center via https://nsidc.org/data/idbmg4/versions/5 (Morlighem et al., 2017). Lastly, the wind fields used in the (Text S5 and Figure S1 in Supporting Information S1) are from the Global Ocean Hourly Reprocessed Sea Surface Wind and Stress from Scatterometer and Model and are available at the Copernicus Marine Service via https://doi.org/10.48670/moi-00185 (Copernicus Marine Service, 2024).

Acknowledgments
We gratefully acknowledge the U.S. National Science Foundation: this work was primarily supported by NSF OCE-1948482 (MN, FS, and DT) with further support by NSF OCE-2023289 (SP), NSF OPP-2042692 (AW), and NSF OCE-1947970 (KF). We thank all the field teams (scientists, technicians and crew) that conducted the survey, with special thanks to James Holte for the CTD data processing, Meg Yoder for the oxygen titrations, and Nicole Abib for compiling the underway bathymetry dataset. We thank Nicholas Foukal for providing the drifter trajectories, Gunnar Voet for the advection-diffusion model, and Ken Zhao for the Ikersuaq fjord sill estimate from BedMachine. Finally, we thank our two reviewers for their constructive, thoughtful, and prompt feedback.

References

Allen, S., & Hickey, B. (2010). Dynamics of advection-driven upwelling over a shelf break submarine canyon. *Journal of Geophysical Research*, *115*(C8). https://doi.org/10.1029/2009JC005731

Amante, C., & Eakins, B. (2009). *ETOPO1 1 Arc-minute global relief model: Procedures, data sources and analysis* [Dataset]. National Geophysical Data Center, NOAA. https://doi.org/10.7289/V5C8276M

Arndt, J. E., Jokat, W., Dorschel, B., Myklebust, R., Dowdeswell, J. A., & Evans, J. (2015). A new bathymetry of the Northeast Greenland continental shelf: Constraints on glacial and other processes. *Geochemistry, Geophysics, Geosystems*, *16*(10), 3733–3753. https://doi.org/10.1002/2015GC005931

Bakker, P., Schmittner, A., Lenaerts, J. T. M., Abe-Ouchi, A., Bi, D., van den Broeke, M. R., et al. (2016). Fate of the Atlantic meridional overturning circulation: Strong decline under continued warming and Greenland melting. *Geophysical Research Letters*, *43*(23), 12–260. https://doi.org/10.1002/2016GL070457

Beaird, N. L., Straneo, F., Le Bras, I., Pickart, R., & Jenkins, W. J. (2023). Glacial meltwater in the current system of Southern Greenland. *Journal of Geophysical Research: Oceans*, *128*(12), e2023JC019658. https://doi.org/10.1029/2023JC019658

Beardsley, R. C., Limeburner, R., & Brechner Owens, W. (2004). Drifter measurements of surface currents near Marguerite Bay on the Western Antarctic Peninsula shelf during austral summer and fall, 2001 and 2002. *Deep Sea Research Part II: Topical Studies in Oceanography*, *51*(17), 1947–1964. https://doi.org/10.1016/j.dsr2.2004.07.031

Bendtsen, J., Rysgaard, S., Carlson, D. F., Meire, L., & Sejr, M. K. (2021). Vertical mixing in stratified fjords near Tidewater outlet glaciers along Northwest Greenland. *Journal of Geophysical Research: Oceans*, *126*(8), e2020JC016898. https://doi.org/10.1029/2020JC016898

Brearley, J. A., Meredith, M. P., Naveira Garabato, A. C., Venables, H. J., & Inall, M. E. (2017). Controls on turbulent mixing on the West Antarctic Peninsula shelf. *Deep Sea Research Part II: Topical Studies in Oceanography*, *139*, 18–30. https://doi.org/10.1016/j.dsr2.2017.02.011

Brearley, J. A., Moffat, C., Venables, H. J., Meredith, M. P., & Dinniman, M. S. (2019). The role of eddies and topography in the export of shelf waters from the West Antarctic Peninsula Shelf. *Journal of Geophysical Research: Oceans*, *124*(11), 7718–7742. https://doi.org/10.1029/2018JC014679

Castelao, R. M., Luo, H., Oliver, H., Rennermalm, A. K., Tedesco, M., Bracco, A., et al. (2019). Controls on the transport of meltwater from the Southern Greenland Ice sheet in the Labrador Sea. *Journal of Geophysical Research: Oceans*, *124*(6), 3551–3560. https://doi.org/10.1029/2019JC015159

Copernicus Marine Service. (2024). Global ocean hourly reprocessed sea surface wind and stress from Scatterometer and Model [Dataset]. *Copernicus Marine*. https://doi.org/10.48670/moi-00185

Couto, N., Martinson, D. G., Kohut, J., & Schofield, O. (2017). Distribution of upper circumpolar deep water on the warming continental shelf of the West Antarctic Peninsula. *Journal of Geophysical Research: Oceans*, *122*(7), 5306–5315. https://doi.org/10.1002/2017JC012840

D'Errico, J. (2006). Surface fitting using gridfit [Software]. https://www.mathworks.com/matlabcentral/fileexchange/8998-surface-fitting-using-gridfit

Dillon, T. M. (1982). Vertical overturns: A comparison of Thorpe and Ozmidov length scales. *Journal of Geophysical Research*, *87*(C12), 9601–9613. https://doi.org/10.1029/JC087iC12p09601

Elipot, S., Sykulski, A., Lumpkin, R., Centurioni, L., & Pazos, M. (2022). Hourly location, current velocity, and temperature collected from Global Drifter Program drifters world-wide [Dataset]. *NOAA National Centers for Environmental Information*. https://doi.org/10.25921/X46C-3620

Evans, J., Ó Cofaigh, C., Dowdeswell, J. A., & Wadhams, P. (2009). Marine geophysical evidence for former expansion and flow of the Greenland Ice Sheet across the North-East Greenland continental shelf. *Journal of Quaternary Science*, *24*(3), 279–293. https://doi.org/10.1002/jqs.1231

Fer, I. (2006). Scaling turbulent dissipation in an Arctic fjord. *Deep Sea Research Part II: Topical Studies in Oceanography*, *53*(1), 77–95. https://doi.org/10.1016/j.dsr2.2006.01.003

Fer, I., Skogseth, R., & Haugan, P. M. (2004). Mixing of the Storfjorden overflow (Svalbard Archipelago) inferred from density overturns. *Journal of Geophysical Research*, *109*(C1). https://doi.org/10.1029/2003JC001968

Fogaren, K. E., & Palevsky, H. I. (2024). Bottle-calibrated Dissolved Oxygen (DO) profiles from US overturning in the Subpolar North Atlantic Program (OSNAP) cruises in 2020 and 2022 (AR45 and AR69-03) [Dataset]. *Biological and Chemical Oceanography Data Management Office (BCO-DMO)*. Retrieved 2024-08-02, from https://www.bco-dmo.org/dataset/933743

Foukal, N. P., & Pickart, R. S. (2023). Moored observations of the West Greenland coastal current along the Southwest Greenland Shelf. *Journal of Physical Oceanography*, *53*(11), 2619–2632. https://doi.org/10.1175/JPO-D-23-0104.1

Freeland, H. J., & Denman, K. L. (1982). A topographically controlled upwelling center off Southern Vancouver Island. *Journal of Marine Research*, *40*, 1069–1093.

Galbraith, P. S., & Kelley, D. E. (1996). Identifying overturns in CTD profiles. *Journal of Atmospheric and Oceanic Technology*, *13*(3), 688–702. https://doi.org/10.1175/1520-0426(1996)013<0688:ioicp>2.0.co;2

Gou, R., Feucher, C., Pennelly, C., & Myers, P. G. (2021). Seasonal cycle of the coastal West Greenland current system between Cape Farewell and Cape desolation from a very high-resolution numerical model. *Journal of Geophysical Research: Oceans*, *126*(5), e2020JC017017. https://doi.org/10.1029/2020JC017017

Harris, P. T., & Whiteway, T. (2011). Global distribution of large submarine canyons: Geomorphic differences between active and passive continental margins. *Marine Geology*, *285*(1), 69–86. https://doi.org/10.1016/j.margeo.2011.05.008

Hautala, S. L., Reid, J. L., & Bray, N. (1996). The distribution and mixing of Pacific water masses in the Indonesian Seas. *Journal of Geophysical Research*, *101*(C5), 12375–12389. https://doi.org/10.1029/96JC00037

Hendry, K. R., Briggs, N., Henson, S., Opher, J., Brearley, J. A., Meredith, M. P., et al. (2021). Tracing glacial meltwater from the Greenland ice sheet to the ocean using gliders. *Journal of Geophysical Research: Oceans*, *126*(8), e2021JC017274. https://doi.org/10.1029/2021JC017274

Hendry, K. R., Huvenne, V. A. I., Robinson, L. F., Annett, A., Badger, M., Jacobel, A. W., et al. (2019). The biogeochemical impact of glacial meltwater from Southwest Greenland. *Progress in Oceanography*, *176*, 102126. https://doi.org/10.1016/j.pocean.2019.102126

Hopwood, M. J., Carroll, D., Browning, T. J., Meire, L., Mortensen, J., Krisch, S., & Achterberg, E. P. (2018). Non-linear response of summertime marine productivity to increased meltwater discharge around Greenland. *Nature Communications*, *9*(1), 3256. https://doi.org/10.1038/s41467-018-05488-8

Howard, L. (1961). Note on a paper of Miles, John W. *Journal of Fluid Mechanics*, *10*(4), 509–512. https://doi.org/10.1017/S0022112061000317

Howard, S. L., Hyatt, J., & Padman, L. (2004). Mixing in the pycnocline over the western Antarctic Peninsula shelf during southern ocean GLOBEC. *Deep Sea Research Part II: Topical Studies in Oceanography*, *51*(17), 1965–1979. https://doi.org/10.1016/j.dsr2.2004.08.002

Howard, S. L., & Padman, L. (2021). Gr1kmTM: Greenland 1 kilometer Tide Model, 2021 [Software]. https://doi.org/10.18739/A2251FM3S

Klinck, J. M. (1996). Circulation near submarine canyons: A modeling study. *Journal of Geophysical Research*, *101*(C1), 1211–1223. https://doi.org/10.1029/95JC02901

Klinck, J. M. (1998). Heat and salt changes on the continental shelf west of the Antarctic Peninsula between January 1993 and January 1994. *Journal of Geophysical Research*, *103*(C4), 7617–7636. https://doi.org/10.1029/98JC00369

Krawczyk, D. W., Kryk, A., Juggins, S., Burmeister, A., Pearce, C., Seidenkrantz, M. S., et al. (2021). Spatio-temporal changes in ocean conditions and primary production in Baffin Bay and the Labrador Sea. *Palaeogeography, Palaeoclimatology, Palaeoecology*, *563*, 110175. https://doi.org/10.1016/j.palaeo.2020.110175

Le Bras, I. A.-A., Straneo, F., Holte, J., & Holliday, N. P. (2018). Seasonality of freshwater in the East Greenland current system from 2014 to 2016. *Journal of Geophysical Research: Oceans*, *123*(12), 8828–8848. https://doi.org/10.1029/2018JC014511

Lin, P., Pickart, R. S., Torres, D. J., & Pacini, A. (2018). Evolution of the freshwater coastal current at the Southern Tip of Greenland. *Journal of Physical Oceanography*, *48*(9), 2127–2140. https://doi.org/10.1175/JPO-D-18-0035.1

Luo, H., Castelao, R. M., Rennermalm, A. K., Tedesco, M., Bracco, A., Yager, P. L., & Mote, T. L. (2016). Oceanic transport of surface meltwater from the southern Greenland ice sheet. *Nature Geoscience*, *9*(7), 528–532. https://doi.org/10.1038/ngeo2708

MacKinnon, J. A., Simmons, H. L., Hargrove, J., Thomson, J., Peacock, T., Alford, M. H., et al. (2021). A warm jet in a cold ocean. *Nature Communications*, *12*(1), 2418. https://doi.org/10.1038/s41467-021-22505-5

Martinson, D. G., & McKee, D. C. (2012). Transport of warm upper circumpolar deep water onto the western Antarctic Peninsula continental shelf. *Ocean Science*, *8*(4), 433–442. https://doi.org/10.5194/os-8-433-2012

Miles, J. W. (1961). On the stability of heterogeneous shear flows. *Journal of Fluid Mechanics*, *10*(4), 496–508. https://doi.org/10.1017/S0022112061000305

Moffat, C., & Meredith, M. (2018). Shelf–ocean exchange and hydrography west of the Antarctic Peninsula: A review. *Philosophical Transactions of the Royal Society A: Mathematical, Physical and Engineering Sciences*, *376*(2122), 20170164. https://doi.org/10.1098/rsta.2017.0164

Moffat, C., Owens, B., & Beardsley, R. C. (2009). On the characteristics of circumpolar deep water intrusions to the West Antarctic Peninsula continental shelf. *Journal of Geophysical Research*, *114*(C5). https://doi.org/10.1029/2008JC004955

Moore, G. W. K., & Renfrew, I. A. (2005). Tip jets and barrier winds: A QuikSCAT climatology of high wind speed events around Greenland. *Journal of Climate*, *18*(18), 3713–3725. https://doi.org/10.1175/JCLI3455.1

Morlighem, M., Williams, C. N., Rignot, E., An, L., Arndt, J. E., Bamber, J. L., et al. (2017). BedMachine v3: Complete bed topography and ocean bathymetry mapping of Greenland from multibeam echo sounding combined with mass conservation. *Geophysical Research Letters*, *44*(21), 11–61. https://doi.org/10.1002/2017GL074954

Mortensen, J., Rysgaard, S., Bendtsen, J., Lennert, K., Kanzow, T., Lund, H., & Meire, L. (2020). Subglacial discharge and its down-fjord transformation in west Greenland fjords with an ice mélange. *Journal of Geophysical Research: Oceans*, *125*(9), e2020JC016301. https://doi.org/10.1029/2020JC016301

Nash, J. D., Alford, M. H., Kunze, E., Martini, K., & Kelly, S. (2007). Hotspots of deep ocean mixing on the Oregon continental slope. *Geophysical Research Letters*, *34*(1). https://doi.org/10.1029/2006GL028170

NOAA National Geophysical Data Center. (2009). ETOPO1 1 arc-minute global relief model [Dataset]. *NOAA National Centers for Environmental Information*. Retrieved from https://www.ncei.noaa.gov/access/metadata/landing-page/bin/iso?id=gov.noaa.ngdc.mgg.dem

Nørgaard-Pedersen, N., & Mikkelsen, N. (2009). 8000 year marine record of climate variability and fjord dynamics from Southern Greenland. *Marine Geology*, *264*(3), 177–189. https://doi.org/10.1016/j.margeo.2009.05.004

Osborn, T. R. (1978). Measurements of energy dissipation adjacent to an island. *Journal of Geophysical Research*, *83*(C6), 2939–2957. https://doi.org/10.1029/JC083iC06p02939

Osborn, T. R. (1980). Estimates of the local rate of vertical diffusion from dissipation measurements. *Journal of Physical Oceanography*, *10*(1), 83–89. https://doi.org/10.1175/1520-0485(1980)010<0083:eotlro>2.0.co;2

Ozmidov, R. V. (1965). On the turbulent exchange in a stably stratified ocean. *Atmospheric and Oceanic Physics*, *8*, 853–860. Retrieved 2024-10-01, from https://search-library.ucsd.edu

Pacini, A., Pickart, R. S., Bahr, F., Torres, D. J., Ramsey, A. L., Holte, J., et al. (2020). Mean conditions and seasonality of the West Greenland boundary current system near Cape Farewell. *Journal of Physical Oceanography*, *50*(10), 2849–2871. https://doi.org/10.1175/JPO-D-20-0086.1

Pacini, A., Pickart, R. S., Bras, I. A. L., Straneo, F., Holliday, N. P., & Spall, M. A. (2021). Cyclonic eddies in the West Greenland boundary current system. *Journal of Physical Oceanography*, *51*(7), 2087–2102. https://doi.org/10.1175/JPO-D-20-0255.1

Rahmstorf, S., Box, J. E., Feulner, G., Mann, M. E., Robinson, A., Rutherford, S., & Schaffernicht, E. J. (2015). Exceptional twentieth-century slowdown in Atlantic Ocean overturning circulation. *Nature Climate Change*, *5*(5), 475–480. https://doi.org/10.1038/nclimate2554

Ribergaard, M. H. (2007). Oceanographic investigations off West Greenland 2006 (Tech. Rep. No. N5339). *Northwest Atlantic Fisheries Organization*. https://www.nafo.int/Portals/0/PDFs/sc/2007/scr07-001.pdf

Schiller-Weiss, I., Martin, T., & Schwarzkopf, F. U. (2024). Emerging influence of enhanced Greenland melting on boundary currents and deep convection regimes in the Labrador and Irminger seas. *Geophysical Research Letters*, *51*(9), e2024GL109022. https://doi.org/10.1029/2024GL109022

Scott, R. M., Brearley, J. A., Naveira Garabato, A. C., Venables, H. J., & Meredith, M. P. (2021). Rates and mechanisms of turbulent mixing in a coastal embayment of the West Antarctic Peninsula. *Journal of Geophysical Research: Oceans*, *126*(5), e2020JC016861. https://doi.org/10.1029/2020JC016861

Shepard, F. P. (1981). Submarine canyons: Multiple causes and long-time persistence. *AAPG Bulletin American Association of Petroleum Geologists*, *65*(6), 1062–1077. https://doi.org/10.1306/03b59459-16d1-11d7-8645000102c1865d

Silvano, A., Holland, P. R., Naughten, K. A., Dragomir, O., Dutrieux, P., Jenkins, A., et al. (2022). Baroclinic Ocean response to climate forcing regulates decadal variability of ice-shelf melting in the Amundsen Sea. *Geophysical Research Letters*, *49*(24), e2022GL100646. https://doi.org/10.1029/2022GL100646

Slater, D. A., & Straneo, F. (2022). Submarine melting of glaciers in Greenland amplified by atmospheric warming. *Nature Geoscience*, *15*(10), 794–799. https://doi.org/10.1038/s41561-022-01035-9

Snow, T., Straneo, F., Holte, J., Grigsby, S., Abdalati, W., & Scambos, T. (2021). More than skin deep: Sea surface temperature as a means of inferring Atlantic water variability on the southeast Greenland continental shelf near Helheim Glacier. *Journal of Geophysical Research: Oceans*, *126*(4), e2020JC016509. https://doi.org/10.1029/2020JC016509

Snow, T., Zhang, W., Schreiber, E., Siegfried, M., Abdalati, W., & Scambos, T. (2023). Alongshore winds force warm Atlantic water toward Helheim glacier in Southeast Greenland. *Journal of Geophysical Research: Oceans*, *128*(9), e2023JC019953. https://doi.org/10.1029/2023JC019953

Spurgin, J. M., & Allen, S. E. (2014). Flow dynamics around downwelling submarine canyons. *Ocean Science*, *10*(5), 799–819. https://doi.org/10.5194/os-10-799-2014

St-Laurent, P., Klinck, J. M., & Dinniman, M. S. (2013). On the role of coastal troughs in the circulation of warm circumpolar deep water on Antarctic shelves. *Journal of Physical Oceanography*, *43*(1), 51–64. https://doi.org/10.1175/JPO-D-11-0237.1

Straneo, F. (2022a). ADCP (Hawaii UHDAS) data as collected during the cruise AR69-03, collaborative Research: Overturning in the Subpolar North Atlantic Program [Dataset]. *Rolling Deck to Repository (R2R)*. https://doi.org/10.7284/153091

Straneo, F. (2022b). Multibeam sonar (Kongsberg EM122) data as collected during the cruise AR69-03, collaborative Research: Overturning in the Subpolar North Atlantic Program [Dataset]. *Rolling Deck to Repository (R2R)*. https://doi.org/10.7284/153098

Straneo, F. (2022c). Multibeam sonar (Kongsberg EM710) data as collected during the cruise AR69-03, collaborative Research: Overturning in the Subpolar North Atlantic Program [Dataset]. *Rolling Deck to Repository (R2R)*. https://doi.org/10.7284/153099

Straneo, F. (2023). OSNAP 2022 Hydrographic cruise: 33VB20220819 [Dataset]. *CCHDO: CLIVAR and Carbon Hydrographic Data Office*. https://doi.org/10.7942/C24H21

Straneo, F., & Heimbach, P. (2013). North Atlantic warming and the retreat of Greenland's outlet glaciers. *Nature*, *504*(7478), 36–43. https://doi.org/10.1038/nature12854

Sutherland, D. A., & Cenedese, C. (2009). Laboratory experiments on the interaction of a buoyant coastal current with a canyon: Application to the East Greenland current. *Journal of Physical Oceanography*, *39*(5), 1258–1271. https://doi.org/10.1175/2008JPO4028.1

Sutherland, D. A., Straneo, F., Stenson, G. B., Davidson, F. J., Hammill, M. O., & Rosing-Asvid, A. (2013). Atlantic water variability on the SE Greenland continental shelf and its relationship to SST and bathymetry. *Journal of Geophysical Research: Oceans*, *118*(2), 847–855. https://doi.org/10.1029/2012JC008354

Swingedouw, D., Houssais, M.-N., Herbaut, C., Blaizot, A.-C., Devilliers, M., & Deshayes, J. (2022). AMOC recent and future trends: A crucial role for oceanic resolution and Greenland melting? *Frontiers in Climate*, *4*. https://doi.org/10.3389/fclim.2022.838310

Thorpe, S. A. (1997). Turbulence and mixing in a Scottish Loch. *Philosophical Transactions of the Royal Society of London - Series A: Mathematical and Physical Sciences*, *286*(1334), 125–181. https://doi.org/10.1098/rsta.1977.0112

Venables, H. J., Meredith, M. P., & Brearley, J. A. (2017). Modification of deep waters in Marguerite Bay, western Antarctic Peninsula, caused by topographic overflows. *Deep Sea Research Part II: Topical Studies in Oceanography*, *139*, 9–17. https://doi.org/10.1016/j.dsr2.2016.09.005

Vernet, M., Ellingsen, I., Marchese, C., Bélanger, S., Cape, M., Slagstad, D., & Matrai, P. A. (2021). Spatial variability in rates of Net Primary Production (NPP) and onset of the spring bloom in Greenland shelf waters. *Progress in Oceanography*, *198*, 102655. https://doi.org/10.1016/j.pocean.2021.102655

Voet, G., Girton, J. B., Alford, M. H., Carter, G. S., Klymak, J. M., & Mickett, J. B. (2015). Pathways, volume transport, and mixing of abyssal water in the Samoan passage. *Journal of Physical Oceanography*, *45*(2), 562–588. https://doi.org/10.1175/JPO-D-14-0096.1

Wood, M., Rignot, E., Fenty, I., An, L., Bjørk, A., van den Broeke, M., et al. (2021). Ocean forcing drives glacier retreat in Greenland. *Science Advances*, *7*(1), eaba7282. https://doi.org/10.1126/sciadv.aba7282

References From the Supporting Information

Atlas, E., Hager, S., Gordon, L., & Park, P. K. (1971). *A practical manual for use of the technicon (trade name) autoanalyzer (trade name) in seawater nutrient analyses; revised. (Tech. Rep. No. AD0730482)*. Oregon State University. Retrieved from https://apps.dtic.mil/sti/citations/AD0730482

Edwards, B., Murphy, D., Janzen, C., & Larson, N. (2010). Calibration, response, and hysteresis in deep-sea dissolved oxygen measurements. *Journal of Atmospheric and Oceanic Technology*, *27*(5), 920–931. https://doi.org/10.1175/2009JTECHO693.1

Egbert, G. D., & Erofeeva, S. Y. (2002). Efficient inverse modeling of Barotropic Ocean tides. *Journal of Atmospheric and Oceanic Technology*, *19*(2), 183–204. https://doi.org/10.1175/1520-0426(2002)019<0183:eimobo>2.0.co;2

Firing, E., & Gordon, R. (1990). Deep Ocean acoustic Doppler current profiling. In *Proceedings of the IEEE fourth working conference on current measurement* (pp. 192–201). https://doi.org/10.1109/CURM.1990.110905

Firing, E., & Hummon, J. M. (2010). Ship-mounted acoustic Doppler current profilers. In *The GO-SHIP repeat hydrography manual: A collection of expert reports and guidelines* (p. 11). International CLIVAR Project Office. Retrieved from https://www.go-ship.org/Manual/Firing_SADCP.pdf

GEBCO Compilation Group. (2020). GEBCO 2020 grid [Dataset]. https://doi.org/10.5285/a29c5465-b138-234d-e053-6c86abc040b9

Gordon, L., Jennings, J., Ross, A., & Krest, J. (1993). A suggested protocol for continuous flow automated analysis of seawater nutrients (Phosphate, Nitrate, Nitrite and Silicic acid) in the WOCE hydrographic Program and the joint Global Ocean fluxes study. *Methods Manual WHPO*, 91.

Palevsky, H., Yoder, M. F., Nicholson, D., & Fogaren, K. E. (2024). Discrete sample measurements of dissolved oxygen, dissolved inorganic carbon, and total alkalinity from US Overturning in the Subpolar North Atlantic Program (OSNAP) cruises in 2020 and 2022 (AR45 and AR69-03) [Dataset]. *Biological and Chemical Oceanography Data Management Office (BCO-DMO)*. https://www.bco-dmo.org/dataset/934025

Uchida, H., Johnson, G. C., & McTaggart, K. E. (2010). CTD oxygen sensor calibration procedures. https://doi.org/10.25607/OBP-1344